Check for updates

Simultaneous capture of methyl orange and chromium(VI) from complex wastewater using polyethylenimine cation decorated magnetic carbon nanotubes as a recyclable adsorbent†

Bo Chen, Wenli Yue, Huinan Zhao, Fengxia Long, Yangrui Cao and Xuejun Pan ᴵᴰ *

Most recently, the continuous deterioration of the aquatic environment triggered by both heavy metals and synthetic organic dyes has imparted serious threats to the ecosphere and drinking water safety. However, it is still extremely challenging to treat complex wastewater containing these two classes of pollutants *via* a one-step method owing to the significant differences in their physicochemical properties. In the current work, versatile magnetic MWCNTs decorated with PEI (denoted as MWCNTs@Fe_3O_4/PEI) was fabricated by a facile, rapid and reproducible strategy and applied to as a robust adsorbent for simultaneously removing methyl orange (MO) and Cr(VI) from aqueous solutions. The physicochemical properties of the as-designed nanohybrid were investigated using various analytical techniques, *i.e.* XRD, FT-IR, SEM, TEM, VSM, zeta potential, *etc.* It was found that the surface charge properties of the MWCNTs as well as its dispersion in aqueous solution were greatly changed after the introduction of PEI molecules. The resulting nanohybrid exhibited attractive adsorption capabilities toward anionic MO and Cr(VI). In the perspective of a mono-pollutant system, the time-dependent adsorption process matched well with a pseudo-second-order kinetics equation, the adsorption isotherm data at r.t. were well fitted by a Langmuir model with maximum monolayer uptake capacity of 1727.6 mg g^{-1} for MO and 98.8 mg g^{-1} for Cr(VI), and the removal process of both pollutants was thermodynamically spontaneous and exothermic. In the MO-Cr(VI) binary system, the uptake of Cr(VI) by the as-prepared adsorbent was evidently enhanced by the presence of MO, while the coexisting Cr(VI) exerted a small negative effect on the sorption of MO; which was attributed to the different adsorption mechanisms of both pollutants on the as-recommend adsorbent. The much better adsorbing performance of the resulting MWCNTs@Fe_3O_4/PEI for MO and Cr(VI) than that of the pristine MWCNTs or the MWCNTs/Fe_3O_4 composite was mainly ascribed to the high surface area of the MWCNTs, the high density of protonated N-rich groups of PEI as well as the excellent dispersion and solubility of the resulting nanocomposites. Moreover, the obtained nanohybrids can be easily recovered after being used by a permanent magnet and still retained high stability and excellent reusability after consecutive adsorption–desorption cycles, implying its great potential in practical applications. Therefore, the as-fabricated MWCNTs@Fe_3O_4/PEI composite could be recommended as a promising candidate adsorbent for the simultaneous capture of MO and Cr(VI) from complex wastewater *via* multiple uptake mechanisms (*e.g.* electrostatic attraction, π–π stacking and hydrogen bonding).

Introduction

The continuous deterioration of water quality has attracted considerable concerns over the world in the past few decades. Various toxic organic and inorganic pollutants have continuously entered the natural waters through the uncontrolled discharge of industrial wastewater. Dyeing effluents, produced from various industrial processes, such as textile, cosmetics, papermaking, plastics, and leather,[1–4] have extremely high organic content and colour strength, drastically inhibit photosynthesis and affect the survival of aquatic fauna and flora; thus imposing great threats on the ecosystem and human health.[5] Moreover, heavy metals (such as Pb(II), Cu(II), Cd(II), and Cr(VI)), which are highly toxic, mutagenic and carcinogenic to living organisms, usually coexist as a mordant in many manufacturing and textile industries.[6,7] The coexistence of both dyes and heavy metals not only impose a more complex risk on

Faculty of Environmental Science and Engineering, Kunming University of Science and Technology, Kunming 650500, P. R. China. E-mail: xjpan@kmust.edu.cn; Fax: +86 871 65920510; Tel: +86 871 65920510

† Electronic supplementary information (ESI) available. See DOI: 10.1039/c8ra08760a

the ecological environment due to the possibility of forming metal complexing dyes, but also inevitably make the efficient treatment of industrial wastewater more challenging ascribed to their different physicochemical properties.[8] Therefore, from the perspectives of environmental protection as well as ecological security, it is very urgent to completely eliminate or minimize the contents of both organic dyes and heavy metal ions in dyeing effluents before discharging them into the receiving water body.

Recently, various techniques, including ion-exchange,[9] biological treatment,[10,11] chemical precipitation,[12,13] membrane separation,[14] catalytic degradation,[15,16] and adsorption,[7,17–20] have been developed to remediate metal- or dye-bearing wastewater. Among them, adsorption is verified to be one of the most promising methods due to its merits of simplicity, effectiveness, and low cost.[21] Generally, the removal performance of the adsorption process is highly dependent on the properties of the adsorptive materials such as the specific surface area, the porous structure, amounts of exposed functional groups, *etc.* Thus, many researchers have made great efforts to develop effective and versatile adsorbents in recent years and numerous novel and effective adsorbents (*i.e.* mesoporous organosilicas,[22] LDHs,[7] MOFs,[23] biochar,[24] carbon nanomaterials,[17,18] bioadsorbent,[8] functionalized magnetic nanoparticles,[19] polymers[25]) have been successfully applied to remove toxic pollutants from contaminated waters. Especially, carbon nanotubes (CNTs) have been widely used as promising adsorptive materials due to their large specific surface areas, excellent stability as well as its broad-spectrum adsorption ability towards different classes of pollutants.[26]

However, pristine CNTs still have several drawbacks for practical application such as lower amounts of functional groups, high surface hydrophobicity, poor selectivity, and difficult solid/liquid separation after being used, which greatly restrain their practical applications in wastewater treatment. To overcome these shortcomings, researchers have modified CNTs by adopting various chemical or physical strategies.[27–32] One of the most efficient methods is to combine CNTs with magnetic components to realize rapid solid/liquid separation under an external magnetic field after adsorption equilibrium was achieved.[26,30,33] However, compared with pristine CNTs, magnetic CNTs usually show relatively unsatisfactory adsorption performance, because the introduction of inert magnetic materials would partially occupy the surface area of the CNTs, leading to significant reduction in the number of accessible active sites for the adsorption of the target pollutants.[33] Moreover, the exposed magnetic components would easily be corroded in a strongly acidic solution, resulting in the poor long-term stability of the proposed adsorbents.

For enhancing the selective adsorption performance as well as the stability of the magnetic CNTs as adsorptive materials, it is necessary to modify its surface with specific materials. Polyethylenimine (PEI), a highly water-soluble polyamine, has gained considerable attention in the field of wastewater remediation owing to the high affinity of its high-density of amine groups on the molecular backbone towards hydrophilic pollutants.[34–36] Several studies have reported that heavy metal

ions can be easily adsorbed by these nitrogen containing moieties through chelation,[37,38] and anionic dyes could also be selectively attracted through electrostatic attraction.[39–41]

Therefore, based on such a hypothesis that hybrids consisting of PEI and magnetic CNTs combine their unique magnetic response, extremely ideal adsorption capability and hydrophilicity, as well as high specific surface area, we are committed to explore PEI decorated magnetic multiwalled carbon nanotubes (denoted as MWCNTs@Fe$_3$O$_4$/PEI) adsorbents integrating excellent uptake performance, rapid magnetic recovery, pH-sensitivity and reusability for the treatment of complex wastewater. Until now, no studies on simultaneously removing MO and Cr(VI) from complex wastewater using MWCNTs@Fe$_3$O$_4$/PEI as adsorbents have been reported. Hence, the purposes of current work was: (i) to design and synthesize an MWCNTs@Fe$_3$O$_4$/PEI composite to improve the drawbacks of pure MWCNTs as adsorptive materials; (ii) to evaluate its selective removal performance for anionic MO and Cr(VI) in their respective mono-pollutant system, including adsorption kinetics, isotherms, thermodynamics, reusability and so on; (iii) to investigate the capability of the proposed sorbent for the simultaneous capture of MO and Cr(VI) from their mixture solution; (iv) to check the practical potential of the as-fabricated adsorbent for the treatment of model wastewater containing both MO and Cr(VI).

Experimental

Materials and reagents

Iron chloride hexahydrate (FeCl$_3$·6H$_2$O), polyethylene glycol (PEG), ethylene glycol (EG), sodium acetate anhydrous (Na$_2$Ac), K$_2$Cr$_2$O$_7$ and methyl orange (MO, 327.33 g mol^{-1}, ≥96%) were of analytical grade and obtained from Aladdin. A branched polyethylenimine (PEI, M.W. = 25 000) was purchased from Sigma-Aldrich. MWCNTs (–COOH content, 1.23 wt%; diameter; 20–30 nm; length, 10–30 μm) were bought from Chengdu Organic Chemicals Co. Ltd, Chinese Academy of Sciences.

Preparation of adsorbents

Preparation of magnetic MWCNTs. The pristine MWCNTs were initially acid treated to remove residual impurities such as metal ions and amorphous carbon. Briefly, 1 g of MWCNTs was mixed with 100 mL of concentrated nitric acid in a three-neck flask with 250 mL capacity and then the suspension was refluxed for 10 h at 60 °C under vigorous stirring. After being naturally cooled, the obtained product was filtered by centrifugation, rinsed thoroughly with adequate deionized water, dried in an oven at 80 °C for 12 h, and stored for use.

Magnetic MWCNTs (MWCNTs@Fe$_3$O$_4$) were obtained *via* a modified solvothermal method as described below[42] Firstly, 1.0 g of FeCl$_3$·6H$_2$O, 4.0 g of Na$_2$Ac, and 1 mL of PEG were dissolved into 60 mL of EG under magnetic stirring. Afterward, 0.3 g of pretreated MWCNTs was suspended into the above solution by ultrasonic irradiation for 30 min to form a homogeneous suspension. Subsequently, the resulting mixture was transferred into a Teflon lined autoclave with 100 mL capacity

and heated at 200 °C for 10 h. Finally, the obtained black products were magnetically isolated, washed several times with copious deionized water, and dried in a vacuum oven at 60 °C for 12 h.

Preparation of PEI modified magnetic MWCNTs composites. Polyethylenimine (PEI) modified magnetic MWCNTs composite (MWCNTs@Fe$_3$O$_4$/PEI) was prepared by combining MWCNTs@Fe$_3$O$_4$ and PEI *via* a simple method. Briefly, different amounts of PEI (0.5 to 7.0 g) were mixed with a 10 mL suspension containing 1 g MWCNTs@Fe$_3$O$_4$. The black mixture was then vigorously stirred for 2 h at room temperature to assemble the PEI molecules onto the magnetic MWCNTs and subsequently dried at 100 °C for 10 h. Finally, the resulting product was washed with copious amounts of deionized water, followed by drying in an oven at 50 °C for 12 h. The schematic diagram for the synthesis of the nanohybrid MWCNTs@Fe$_3$O$_4$/PEI is shown in Scheme 1.

Characterization of adsorbents

The surface morphology, structural composition and physico-chemical characteristics of the samples were investigated using various analytical techniques including SEM (scanning electron microscope), TEM (transmission electron microscope), EDS (energy dispersive X-ray spectrum), FT-IR (Fourier transform infrared spectroscopy), XRD (X-ray diffraction), TGA (thermal gravimetric analysis), VSM (vibrating sample magnetometer), *etc.* The FT-IR spectra of the samples in the region of 4000–400 cm^{-1} were obtained with a Magna-IR 750 spectrometric analyser (Nicolet Co., USA). Typical XRD patterns over a 2θ range of 10–80° were acquired on a Bruker D8 Advance X-ray diffractometer (Bruker Inc., Germany). SEM images and EDS spectra of samples were obtained using a NoVa™ Nano SEM 250 (FEI Co., USA). TEM images were recorded using an FEI Tecnai G20 microscope (FEI Co., USA). TGA analysis was conducted *via* TAQ 600 instrument (TA Instruments, Inc., USA) under a N$_2$ atmosphere. The magnetization curves of the samples at room temperature were measured by a VSM (Quantum Design, Inc., USA). The pH-dependent surface charges of the samples at different pH values were determined using a Malvern 3600 Zetasizer (Malvern Instruments Ltd., UK).

Batch adsorption experiments in a mono-pollutant system

To investigate the adsorption kinetics, thermodynamics, isotherms, and effect of pH on the adsorption of each pollutant by the as-prepared adsorbent, all batch experiments in the mono-component system were conducted in glass conical bottles with 100 mL capacity by shaking at 150 rpm in an air bath shaker and the experiments were performed in duplicate. The experimental details for each batch experiment are shown in ESI.† Afterwards, the uptake amounts at time t and equilibrium for each pollutant were calculated by the following equations:

$$q_t = \frac{(C_0 - C_t)V}{m} \tag{1}$$

$$q_e = \frac{(C_0 - C_e)V}{m} \tag{2}$$

where q_e (mg g^{-1}) and q_t (mg g^{-1}) represent equilibrium adsorption amount and that of time t, respectively; C_0 (mg L^{-1}), C_t (mg L^{-1}), and C_e (mg L^{-1}) represent the initial, residual, and equilibrium concentration of the adsorbate, respectively. V (mL) is the volume of the adsorbate solution and m (g) represents the dosage of the adsorbent.

Adsorption isotherms in a binary system

In order to investigate the simultaneous removal performance of the as-prepared MWCNTs@Fe$_3$O$_4$/PEI composite adsorbent towards MO and Cr(VI), as well as the mutual effects in a complex system, adsorption isotherms of the MWCNTs@Fe$_3$O$_4$/PEI toward individual pollutants (Cr(VI) and MO) at 25 °C in a MO-Cr(VI) binary system were performed and compared with those isotherms obtained in a mono-pollutant system. The detailed adsorption conditions in a binary system were specifically described in ESI† and the adsorption-separation process in the binary system is illustrated in Scheme 2.
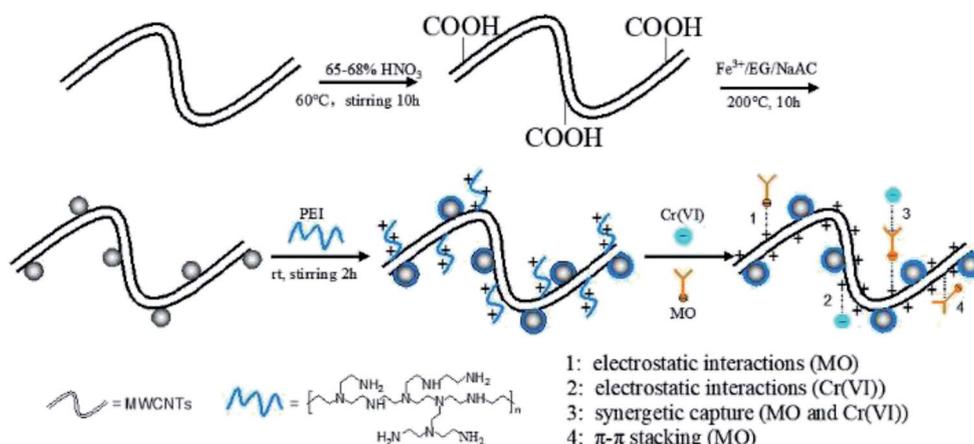
Scheme 1 Synthesis of MWCNTs@Fe$_3$O$_4$/PEI composite and the proposed adsorption mechanisms.
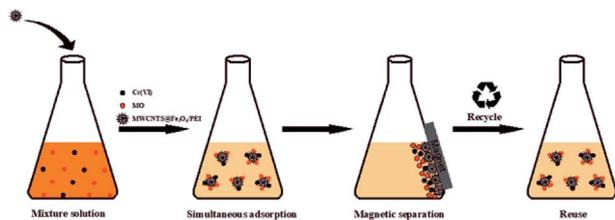
Scheme 2 Schematic diagram for simultaneous capture of MO and Cr(VI) in MO–Cr(VI) binary system.

Fig. 1 SEM images of MWCNTs (a), MWCNTs@Fe$_3$O$_4$ (b), MWCNTs@Fe$_3$O$_4$/PEI (c), and TEM images of MWCNTs (d), MWCNTs@Fe$_3$O$_4$ (e), MWCNTs@Fe$_3$O$_4$/PEI (f).

Regeneration and stability of resulting adsorbent

The regeneration and stability of the as-obtained adsorbent for the uptake of MO and Cr(VI) were tested by checking the cycle number-dependent adsorption capacities for 200 mg L^{-1} MO and 50 mg L^{-1} Cr(VI), respectively. The details are as follows; the saturated adsorbents with MO or Cr(VI) were first dispersed into a 30 mL NaOH solution (0.5 mol L^{-1}) by sonication for 10 min. After that, the solid material was separated from the eluent with a permanent magnet, followed by washing thoroughly with deionized water, and then reused in the next cycle of adsorption experiments.

Evaluation of MWCNTs@Fe$_3$O$_4$/PEI for a model effluent

The treatment performance of MWCNTs@Fe$_3$O$_4$/PEI for model wastewater was evaluated for its practical potential. On the basis of OECD guidelines for chemicals testing,[8] a synthetic sewage consisting of peptone (160 mg), meat extract (110 mg), K$_2$HPO$_4$ (28 mg), urea (30 mg), NaCl (7 mg), CaCl$_2$·2H$_2$O (4 mg), MgSO$_4$·7H$_2$O (2 mg), and tap water (1 L) was prepared and then applied as solvent for preparing the model textile effluent with 50 mg L^{-1} Cr(VI) or 200 mg L^{-1} MO, respectively. The adsorption was conducted by blending 15 mg of the adsorbent with 30 mL of simulated wastewater (the ratio of solid to liquid, 0.5 g L^{-1}) at an initial solution pH of 3.0. After an adsorption equilibrium was achieved, the solid was facilely isolated by a permanent magnet and the residual concentration of target adsorbate in the supernatant was determined using UV-Vis spectroscopy. Then the separated adsorbents were successfully treated by using 30 mL of eluent and washed with adequate deionized water. Finally, the regenerated MWCNTs@Fe$_3$O/PEI was used again for the next run of the adsorption process. The adsorption–desorption cycles were repeated twice to evaluate the duration of the as-synthesized adsorbent in practical application.

Results and discussion

Characterization of adsorbents

The morphology of the samples can be observed from the SEM images shown in Fig. 1a–c. For pristine MWCNTs, it is clearly observed that numerous tubes interconnected to form a porous network due to the excellent flexibility of individual nanotube. As for MWCNTs@Fe$_3$O$_4$, the monodispersed Fe$_3$O$_4$ nanopar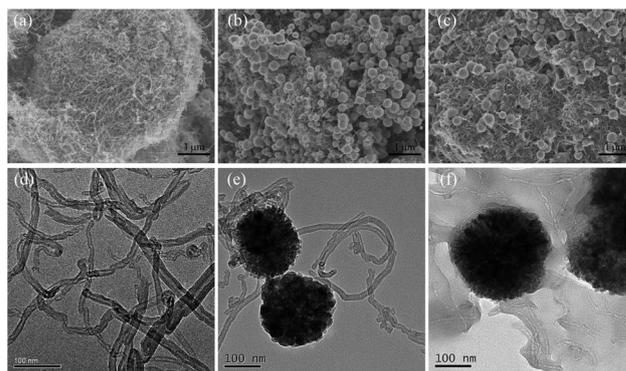ticles were evenly attached on the surface of MWCNTs. After the introduction of PEI, the tubes aggregate together to form a more ordered network, which is conducive to the adsorption proceeding. Synchronously, the EDS spectra were recorded to verify the surface composition of the MWCNTs@Fe$_3$O$_4$/PEI (Fig. S1†). It is clear that, except for C (70.28 at%), N (8.98 at%) and O (15.91 at%) were the abundant elements, which is consistent with our expectations.

TEM images of the samples shown in Fig. 1d–f indicated that highly dispersed MWCNTs are with a tubular hollow structure and with an average diameter of 20–30 nm. Magnetic Fe$_3$O$_4$ nanospheres with an average size of 150–200 nm were successfully decorated on the tips of the MWCNTs to form tadpole-like nanocomposites through solvothermal treatment. A dense and transparent polymeric layer was clearly observed on the surfaces of both the MWCNTs and Fe$_3$O$_4$, indicating that the PEI molecules were successfully introduced into the hybrid.

The XRD results of the samples are depicted in Fig. 2a. The diffraction peak at $2\theta = 26.4°$ from the (002) plane of the MWCNTs was observed in all three samples, indicating that the crystalline structure of the MWCNTs remains intact and was not destroyed during the whole preparation process.[43] Compared with the pristine MWCNTs, the intensity of this peak in the other two samples significantly decreased due to the deposition of Fe$_3$O$_4$ nanoparticles and decoration of PEI molecules on the surface. The peaks of Fe$_3$O$_4$ nanoparticles with the cubic spinel structure at $2\theta = 30.1°$ (220), 35.5° (311), 43.1° (400), 53.4° (422), 57.0° (511) and 62.6° (440) appeared in both MWCNTs@Fe$_3$O$_4$ and MWCNTs@Fe$_3$O$_4$/PEI, further confirming the presence of the magnetite component in the composites. By comparison, the intensity of each peak for the MWCNTs@Fe$_3$O$_4$/PEI decreased slightly after PEI modification, suggesting the successful grafting of PEI molecules onto the magnetic MWCNTs.

FT-IR spectra of the resulting samples were shown in Fig. 2b. For MWCNTs, the absorption bands at *ca.* 3417, 1633, and 1395 cm^{-1} are from asymmetrical and symmetrical vibrations of the carboxyl group.[44] The strong peak at around 587 cm^{-1} in both MWCNTs@Fe$_3$O$_4$ and MWCNTs@Fe$_3$O$_4$/PEI was attributed to the stretching mode of Fe–O bonds in the Fe$_3$O$_4$ nanoparticles.[45] Owing to the introduction of the PEI molecules,
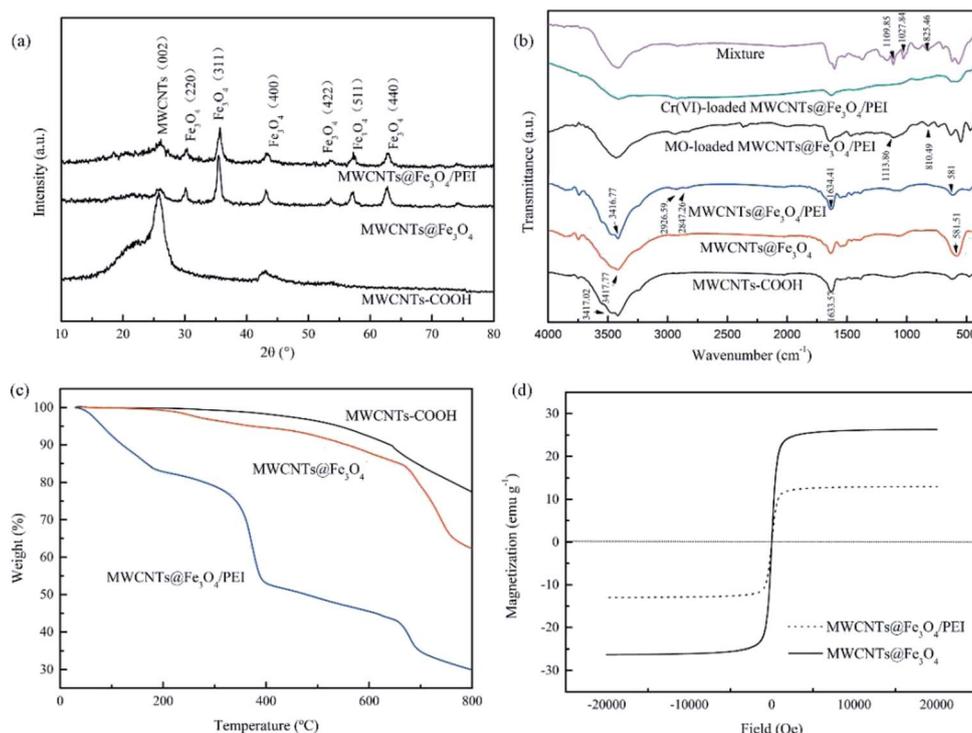
Fig. 2 Characterization of the samples. XRD patterns (a); FT-IR spectra (b); TGA curves (c); Magnetization curves (d).

some newly appeared peaks were observed in the FT-IR spectrum of MWCNTs@Fe$_3$O$_4$/PEI. The absorption band at 3416 cm^{-1}, overlapped with the –OH of the MWCNTs and was much stronger than that of the MWCNTs@Fe$_3$O$_4$, from the stretch vibration of N–H bond in PEI. The two peaks at 2927 and 2847 cm^{-1} are due to the symmetric and asymmetric stretches of the –CH$_2$ groups in PEI, respectively.[45]

TGA curves of the samples were depicted in Fig. 2c. Obviously, the MWCNTs and MWCNTs@Fe$_3$O$_4$ are thermally stable at a temperature below 200 °C. After that, the slight weight loss of about 5 wt% for the MWCNTs@Fe$_3$O$_4$ and 1.0 wt% for the MWCNTs were observed in the temperature region of 200–350 °C. The weight loss from 350 to 800 °C was from thermal decomposition of the MWCNTs. For MWCNTs@Fe$_3$O$_4$/PEI, the weight loss of about 16.0 wt% below 200 °C was attributed to deintercalation of water in the sample. Over the temperature range of 200–300 °C, about 9.2 wt% of weight loss for MWCNTs@Fe$_3$O$_4$/PEI was observed. From 300 to 400 °C, the MWCNTs@Fe$_3$O$_4$/PEI showed a rapid weight loss (ca. 20.8 wt%), which was due to the decomposition of PEI molecules.[36] Decomposition of MWCNTs from 400 to 650 °C caused a further weight loss of the MWCNTs, MWCNTs@Fe$_3$O$_4$, and MWCNTs@Fe$_3$O$_4$/PEI. At a higher temperature above 650 °C, Fe$_3$O$_4$ slowly decomposed due to high thermal stability metal oxides.[46] Based on the aforementioned results, the loading mass of PEI on MWCNTs@Fe$_3$O$_4$/PEI was calculated to be ca. 20.8 wt% when 2.4 g of PEI was used for the preparation of the target adsorbent.

The magnetization curves in Fig. 2d indicated that both samples with Fe$_3$O$_4$ magnetite were superparamagnetic. The values of the saturation magnetization were determined to be 26.3 emu g^{-1} for MWCNTs@Fe$_3$O$_4$ and 13.0 emu g^{-1} for MWCNTs@Fe$_3$O$_4$/PEI, respectively. Compared with MWCNTs@Fe$_3$O$_4$, the magnetism for MWCNTs@Fe$_3$O$_4$/PEI was obviously decreased, manifesting that large amounts of nonmagnetic PEI molecules were introduced into the nanocomposites. However, MWCNTs@Fe$_3$O$_4$/PEI could still be easily isolated from treated wastewater under a magnetic field within several seconds. The adequate magnetic response of the resulting adsorbents meets the demand of fast solid/liquid separation after an adsorption equilibrium was achieved.[47]

Adsorption performance of MWCNTs@Fe$_3$O$_4$/PEI in mono-pollutant system

Effect of solution pH on uptake performance. Initial solution pH is one of the most important factors influencing the adsorption behaviour of ionizable compounds, because the solution pH not only affects the ionization state of the adsorbates but also determines the surface charge of adsorbents.[45] Thus, the effects of solution pH varying from 2 to 11 on the uptake capacities of three different adsorbents for anionic MO and Cr(VI) were investigated in the present work. It is obvious from Fig. 3 that the removal of MO and Cr(VI) by the as-obtained sorbents was highly dependent on the solution pH values. MWCNTs@Fe$_3$O$_4$/PEI showed much higher adsorption capacities than the other two adsorbents within the investigated pH range for MO and Cr(VI) removal, implying that the surface modification with PEI is an effective strategy to improve the
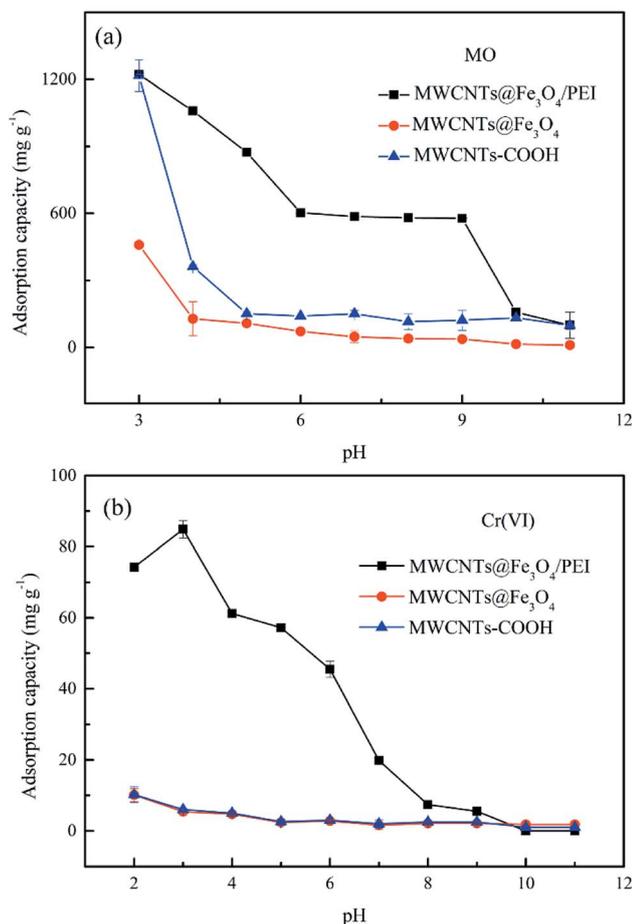
Fig. 3 Effect of solution pH on uptake of MO (a) and Cr(VI) (b) by different adsorbents (conditions: initial dye concentration, 200 mg L^{-1} for MO, 50 mg L^{-1} for Cr(VI); adsorbent dosage, 3 mg for MO, 10 mg for Cr(VI); solution pH, 3–11; contact time, 6 h; temperature, 25 °C; and agitation speed, 150 rpm).

adsorption performance of MWCNTs towards anionic compounds. At a pH below 6, the adsorption capacity of the MWCNTs@Fe$_3$O$_4$/PEI for MO declined sharply with the raising of pH values. Over a pH range of 6–9, the adsorption process is almost not affected by the solution pH. At pH above 9, the removal of MO on the MWCNTs@Fe$_3$O$_4$/PEI is significantly depressed.

The uptake behaviour of MO and Cr(VI) by the three different sorbents at various pH values can be further explained using plots of the zeta potentials *versus* pH values shown in Fig. S4.† As can be seen, because of the introduction of PEI molecules the pH$_{pzc}$ of MWCNTs@Fe$_3$O$_4$/PEI is up to *ca.* 11.5, which is much higher than those of MWCNTs (pH$_{pzc}$ of *ca.* 3.5) and MWCNTs@Fe$_3$O$_4$ (pH$_{pzc}$ of *ca.* 9.0). This indicates that in a wide pH region the surface of as-prepared MWCNTs@Fe$_3$O$_4$/PEI is positively charged. At a lower pH, large amounts of amine and imine groups on MWCNTs@Fe$_3$O$_4$/PEI are protonated to form positively charged active sites conducive to the uptake of anionic compounds through electrostatic attraction, resulting in an improved adsorption capacity toward MO and Cr(VI). Whereas, at higher pH values, MWCNTs@Fe$_3$O$_4$/PEI surfaces

are increasingly deprotonated and competitive uptake from OH$^-$ is gradually enhanced, leading to decline in the adsorption capacity. However, it was observed that adsorption of MO in the pH of 6–9 is highly independent of the solution pH where electrostatic attraction between MO and resulting adsorbent is greatly shielded, demonstrating that the π–π EDA interaction between the localized π-electron in the conjugate aromatic rings of the CNTs and MO molecules plays a major role in the sorption of MO in this region. For the uptake of Cr(VI) by MWCNTs@Fe$_3$O$_4$/PEI, the q_e values declined sharply with an increase of the solution pH, indicating that the electrostatic attraction between the anionic Cr(VI) and cationic surfaces of the MWCNTs@Fe$_3$O$_4$/PEI is the dominant mechanism for the occurance of the adsorption. It is observed that, besides an extremely low q_e of Cr(VI) at a low pH, uptake of Cr(VI) by MWCNTs and MWCNTs@Fe$_3$O$_4$ is highly independent on the solution pH and the adsorption of Cr(VI) by these two adsorbents is almost negligible at neutral and alkaline conditions, manifesting that no specific adsorption sites are available for Cr(VI) uptake on these two adsorbents. Additionally, intermolecular hydrogen bonds are not involved in the adsorption process because the uptake of both MO and Cr(VI) follows the monolayer coverage mechanism and higher temperatures are more favourable for adsorption, which is contradictory to multilayer adsorption caused by intermolecular hydrogen bonds between adsorbate molecules.[48] Therefore, it can be easily concluded from the aforementioned discussion that the highly efficient adsorption removal of MO was mainly driven by electrostatic interaction while the π–π EDA interaction has a secondary role in the adsorption process, and Cr(VI) was mainly adsorbed by electrostatic interaction. Hydrogen bonding between MO (or HCrO$_4^-$) and the residual carboxyl groups on the edges of the CNTs may also participate in the removal of MO and Cr(VI) on the as-obtained adsorbent. The proposed adsorption mechanisms are shown in Scheme 1.

Adsorption kinetics

Time-dependent adsorption of MO by MWCNTs, MWCNTs@Fe$_3$O$_4$, and MWCNTs@Fe$_3$O$_4$/PEI was carried out with an initial concentration of 200 mg L^{-1} at 298 K. Also similar experiments were conducted for 50 mg L^{-1} of Cr(VI) using MWCNTs@Fe$_3$O$_4$/PEI as the adsorbent. The adsorption kinetics data shown in Fig. 4(a and b) indicated that compared with MWCNTs and MWCNTs@Fe$_3$O$_4$, MWCNTs@Fe$_3$O$_4$/PEI showed a much higher sorption affinity toward MO; this is ascribed to the synergetic effect of PEI with a high cationic charge density and the MWCNTs with high surface area towards MO uptake. It is clear that both MO and Cr(VI) were rapidly adsorbed by the MWCNTs@Fe$_3$O$_4$/PEI in the first stage because of the fast mass transfer from the significant concentration difference of adsorbates between the bulk solution and the surface of adsorbent.

To get further insight into the uptake kinetics of MWCNTs@Fe$_3$O$_4$/PEI for MO and Cr(VI), pseudo-first-order (eqn (3)) and pseudo-second-order kinetics (eqn (4)) models were exploited to simulate the experimental data:
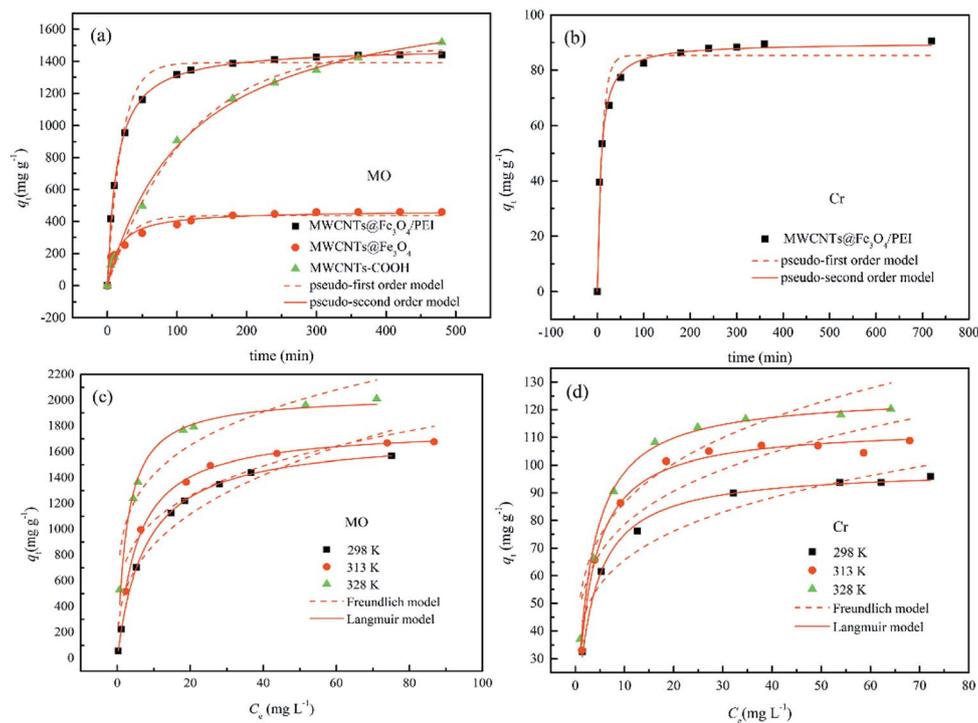
Fig. 4 Adsorption kinetics of MO on three different adsorbents (a), adsorption kinetics of Cr(VI) on MWCNTs@Fe$_3$O$_4$/PEI adsorbent (b), adsorption isotherms curves of MO (c) and Cr(VI) (d) on MWCNTs@Fe$_3$O$_4$/PEI (Conditions: 60–330 mg L^{-1} for MO, 10–90 mg L^{-1} for Cr(VI); adsorbent dosage, 3 mg for MO, 10 mg for Cr(VI); solution pH, 3; contact time, 6 h for MO, 4 h for Cr(VI); temperature, 25–55 °C; and agitation speed, 150 rpm).

$$q_t = q_e(1 - e^{-k_1 t}) \tag{3}$$

$$q_t = \frac{q_e^2 k_2 t}{1 + q_e k_2 t} \tag{4}$$

where q_e (mg g^{-1}) represents the equilibrium adsorption capacity; q_t (mg g^{-1}) is the amount of MO and Cr(VI) adsorbed at time t (min); k_1 (min^{-1}) and k_2 (g mg^{-1} min^{-1}) denote adsorption rate constants of pseudo-first-order and pseudo-second-order kinetics, respectively.

The simulated kinetic parameters are presented in Table 1. By comparison, the pseudo-second-order kinetics better fitted the adsorption of MO and Cr(VI) on MWCNTs@Fe$_3$O$_4$/PEI because of the higher correlation coefficients (R^2), suggesting that the chemical adsorption was the rate-limiting step for the uptake of MO and Cr(VI).[49] Moreover, the calculated q_e values from the pseudo-second-order kinetics model were much nearer to the experimental ones. Therefore, the pseudo-first-order kinetics was not suitable for explaining the rate processes.

Adsorption isotherms

To maximize adsorption capability of MWCNTs@Fe$_3$O$_4$/PEI toward MO and Cr(VI), adsorption isotherms at three different temperatures were performed at a pH of 3.0 over an initial concentration range of 60–330 mg L^{-1} for MO and 10–90 mg L^{-1} for Cr(VI), respectively. The obtained equilibrium data were simulated by using the Langmuir and Freundlich equations, which are two well-known isotherm models. The Langmuir model assumes that adsorbents surface are energetically identical and one active site can only be occupied by one adsorbate molecule,[50] revealing that a monolayer of adsorbates covers the surface of the homogeneous adsorbent. The nonlinear form of the Langmuir isotherms model is as follows:

$$q_e = \frac{q_{max} K_L C_e}{1 + K_L C_e} \tag{5}$$

where q_e (mg g^{-1}) and q_m (mg g^{-1}) represent the equilibrium and maximum monolayer adsorption capacity, respectively. C_e (mg L^{-1}) is equilibrium concentration of adsorbate and K_L (L mg^{-1}) is Langmuir equilibrium constant.

The Freundlich model as an empirical equation is used to characterize the heterogeneity of the adsorbents, which is represented in eqn (6).[51]

$$q_e = K_F C_e^{1/n} \tag{6}$$

where K_F and n are the Freundlich constants associated with adsorption capacity and adsorption intensity. The magnitude of

Table 1 Kinetics parameters for adsorption of MO and Cr(VI) by MWCNTs@Fe$_3$O$_4$/PEI

Adsorbate	q_{exp}	Pseudo-first-order kinetic model			Pseudo-second-order kinetic model		
		q_{cal}	k_1	R^2	q_{cal}	k_2	R^2
MO	1440.4	1390	0.0506	0.9807	1489	0.0001	0.9997
Cr(V)	90.6	85.4	0.0952	0.9616	89.9	0.0016	0.9969

the n values indicates whether the adsorption is easy ($2 \leq n < 10$), difficult ($n < 1$) or somewhat difficult ($1 \leq n < 2$).[52]

The fitted isotherms curves are shown in Fig. 4(c and d). It is clear that because of the strong driving force derived from the large concentration difference between the adsorbate and the adsorbent,[53,54] the adsorption capacities increased sharply at the initial stage with increasing adsorbate concentration, slowed down afterward, and finally almost reached equilibrium. The parameters concerning the isotherms are listed in Table 2. By comparing the correlation coefficients (R^2), the experimental data were well fitted by the Langmuir model instead of the Freundlich model, demonstrating that the capture of both MO and Cr(VI) by MWCNTs@Fe$_3$O$_4$/PEI is by the monolayer mode. The monolayer adsorption capacities of MO and Cr(VI) at 298 K are calculated to be 1727.6 and 98.8 mg g^{-1}, respectively. It was clearly observed that the q_{max} values increased from 1727.6 to 2040.1 mg g^{-1} for MO, and rose rased from 98.8 to 125.7 mg g^{-1} for Cr(VI) by varying the temperature from 298 to 328 K, suggesting that the uptake process of MO and Cr(VI) by MWCNTs@Fe$_3$O$_4$/PEI was thermodynamically endothermic in nature. The n values of Freundlich model were higher than 2, suggesting that both MO and Cr(VI) were adsorbed by MWCNTs@Fe$_3$O$_4$/PEI easily.

Also, the separation factor R_L was applied to evaluate whether the adsorption of target pollutants is favorable ($0 < R_L < 1$), unfavorable ($R_L > 1$), linear ($R_L = 1$) or irreversible ($R_L = 0$).[55]

$$R_L = \frac{1}{1 + K_L C_0} \tag{7}$$

where K_L (L mg^{-1}) is the Langmuir constant, C_0 (mg L^{-1}) is the initial concentration of adsorbate.

As is shown in Table 2, over the investigated concentration range the R_L values were 0.0078–0.1133 for MO and 0.0313–0.2418 for Cr(VI), indicating that the adsorption process of the resulting adsorbent towards the investigated adsorbates was favourable. Note that the extremely high adsorption capacity of MWCNTs@Fe$_3$O$_4$/PEI for MO was mainly assigned to the synergistic effect of multiple uptake mechanisms (such as electrostatic attraction, π–π stacking and hydrogen bond) contributed from the PEI molecules with a high cationic charge density, MWCNTs with an aromatic planar structure as well as residual oxygen-containing groups on MWCNTs.

In addition, by comparing the adsorption performance of the resulting adsorbent with that of the other adsorbents reported in the previous publications (Table 3), it was clearly found that the uptake capacities of MWCNTs@Fe$_3$O$_4$/PEI toward MO and Cr(VI) are much higher than or comparable to those of most reported adsorbents. Thus, MWCNTs@Fe$_3$O$_4$/PEI can be considered to be a promising adsorbent for the treatment of MO- or Cr(VI)-bearing wastewater.

Adsorption thermodynamics

To better understand the adsorption process, the thermodynamic parameters (such as ΔG, ΔH and ΔS) for adsorption of MO and Cr(VI) can be calculated from the equilibrium data obtained over the temperature range of 298 to 313 K according to eqn (8), (9) and (10).[68]

$$\Delta G = -RT \ln K_d \tag{8}$$

$$\ln K_d = \frac{\Delta S}{R} - \frac{\Delta H}{RT} \tag{9}$$

$$K_d = \frac{q_e}{C_e} \tag{10}$$

where R (8.314 J mol^{-1} K^{-1}) and T (K) are the gas constant and absolute temperature, respectively. K_d is the equilibrium constant which can be obtained via eqn (10). C_e (mg L^{-1}) and q_e (mg g^{-1}) is equilibrium concentration of adsorbate in aqueous solution and equilibrium uptake amount of the adsorbate, respectively. ΔS and ΔH can be obtained from intercept and slope of plotting of ln K_d versus $1/T$, respectively.

The values for the thermodynamic parameters are listed in Table 4. ΔG values are negative and decrease with increasing temperature, revealing that the uptake of MO and Cr(VI) by MWCNTs@Fe$_3$O$_4$/PEI is a thermodynamically spontaneous process and higher temperature is more conducive to the adsorption proceeding. Positive values of ΔH indicates that the adsorption processes is endothermic in nature and the positive values of ΔS suggest a certain degree of freedom increase on the solid/liquid interface during adsorption of MO and Cr(VI).[69]

Regeneration, stability and reusability of adsorbent

It is extremely crucial to determine the regeneration, stability and reusability of a promising adsorbent for real wastewater treatment. Based on the fact that a higher solution pH hinders the uptake of MO and Cr(VI) in this study, it can be deduced that the alkaline solution (i.e. sodium hydroxide) could be chosen as

Table 2 Langmuir and Freundlich parameters for adsorption of MO and Cr(VI) on MWCNTs@Fe$_3$O$_4$/PEI

| Adsorbate | T (K) | q_{max} | Langmuir model | | | | Freundlich model | | |
			K_L	R^2	R_L		K_F	n	R^2
MO	298	1727.6	0.1305	0.9998	0.0227–0.1133		396.7	2.89	0.9213
	313	1786.1	0.1856	0.9979	0.0161–0.0824		612.3	4.15	0.8914
	328	2040.1	0.3855	0.9859	0.0078–0.0414		876.5	4.74	0.8914
Cr(VI)	298	98.8	0.3135	0.9953	0.0342–0.2418		40.1	4.68	0.9109
	313	114.0	0.3419	0.9919	0.0315–0.2263		48.9	4.85	0.8269
	328	125.7	0.3438	0.9913	0.0313–0.2253		52.3	4.58	0.8753

Table 3 Comparison of adsorption performance of resulting adsorbent with previously reported adsorbents for MO and Cr(VI) uptake

Type of adsorbent	Pollutant	q_{max} (mg g^{-1})	Experimental conditions	Equilibrium time (min or h)	Ref.
PEI modified persimmon tannin bioadsorbent	MO	225.7	pH = 4.0; T = 323 K	120 min	56
Hierarchical GOs/Fe$_3$O$_4$/PANI magnetic composites	MO	585.0	pH = 4.0; T = 298 K	*ca.* 300 min	57
Fe$_3$O$_4$/MIL-101(Al$_{0.9}$ Fe$_{0.1}$)/NH$_2$	MO	355.8	pH = 6.0; T = 323 K	150 min	58
Co/Cr-codoped ZnO nanoparticle	MO	1057.9	pH = 7.0; T = 298 K	Within 150 min	59
CoFe$_2$O$_4$/MgAl-LDO	MO	1219.5	pH = 6.0; T = 298 K	*ca.* 360 min	60
MWCNTs@Fe$_3$O$_4$/PEI	MO	1727.6	pH = 3.0; T = 298 K	240 min	This study
Biochar modified by Fe$_3$O$_4$@SiO$_2$–NH$_2$	Cr(VI)	27.2	pH = 1.0; T = 303 K	300 min	61
Polydopamine@zeolitic idazolate frameworks-8 microspheres	Cr(VI)	136.6	pH = 5.0; T = 293 K	1440 min	62
NiFe$_2$O$_4$/ZnAl LDH/EDTA	Cr(VI)	77.2	pH = 6.0; T = 318 K	Within 120 min	63
Boehmite/PVA composite membrane	Cr(VI)	36.4	pH = 5.5; T = 298 K	360 min	64
PEI functionalized halloysite nanotubes	Cr(VI)	102.5	pH = 2.0; T = 328 K	1200 min	65
Mesoporous silica magnetite nanoparticles modified by 3-aminopropyltriethoxysilane	Cr(VI)	34.3	pH = 2.0; T = 298 K	120 min	66
Poly(ethylene-*co*-vinyl alcohol) functional nanofiber membranes	Cr(VI)	90.7	pH = 2.0; T = 298 K	120 min	67
MWCNTs@Fe$_3$O$_4$/PEI	Cr(VI)	98.8	pH = 3.0; T = 298 K	240 min	This study

Table 4 Thermodynamic parameters for adsorption of MO and Cr(VI) on MWCNTs@Fe$_3$O$_4$/PEI

Adsorbate	ΔH (KJ mol^{-1})	ΔS (J mol^{-1} K^{-1})	ΔG (KJ mol^{-1}) 298 K	313 K	328 K
MO	9.269	60.99	−9.094	−9.755	−10.77
Cr(VI)	13.199	69.837	−7.729	−8.403	−9.849

an efficient desorption eluent for MO and Cr(VI) adsorbed by MWCNTs@Fe$_3$O$_4$/PEI adsorbent. As presented in Fig. 5, MO and Cr(VI) can be easily desorbed from the target adsorbent by using 0.5 M NaOH and no obvious drop in the removal efficiency was observed even after three conservative adsorption–desorption cycles, confirming the excellent stability of the as-prepared adsorbent for MO removal. However, in the case of Cr(VI), the uptake rate decreased by approximate 10% after being subject to five sorption–desorption cycles, which is probably acceptable for treatment of industrial scale wastewater. Thus, the excellent regeneration, stability and reusability of MWCNTs@Fe$_3$O$_4$/PEI make it a potential adsorbent for MO and Cr(VI) capture from wastewater. Besides the aforementioned advantages, this adsorbent has other merits such as simple and mild preparation process, easy recyclability, low adsorbent dosage, no secondary pollution, *etc.* These characteristics are of great importance for the simultaneously capturing other anionic organic and inorganic pollutants in real wastewaters.

Simultaneous capture of MO and Cr(VI) in MO-Cr(VI) binary system

To check the simultaneous removal performance of the as-prepared adsorbent in practical applications as well as the mutual effect between co-existing pollutants, the isotherms for MO and Cr(VI) adsorption by MWCNTs@Fe$_3$O$_4$/PEI in binary systems were carried out in present work. It can be clearly observed from Fig. 6 that the removal of Cr(VI) by the adsorbent was greatly promoted by the presence of MO and the q_e value of Cr(VI) gradually increased with increasing MO concentration from 0 to 40 mg L^{-1}. This may be due to that the protonated –N(CH$_3$)$_2$ portion of MO that could provide additional sorption sites for Cr(VI) uptake *via* electrostatic attraction under acidic conditions, thus increasing the uptake amount of Cr(VI) by MWCNTs@Fe$_3$O$_4$/PEI. For MO$^-$, both the electrostatic interaction and the π–π EDA interaction play a very important role in the adsorption process. When MO and Cr(VI) coexist, Cr(VI) with a smaller molecular size is more likely to be preferentially adsorbed on the surface of the protonated adsorbent *via* an electrostatic mechanism, occupying part of the active sites available for MO, resulting in a decrease in the adsorption amount of MO by the as-proposed adsorbent. The adsorbed HCrO$_4^-$ monolayer could not further adsorb MO by electrostatic attraction, which may be due to that the single anion charge of HCrO$_4^-$ has reacted with the protonated N atom on the adsorbent surface and the adsorbed Cr(VI) could not provide an extra active site for MO uptake.

Moreover, the mutual effects between each pollutant in the binary system were evaluated by using the ratio of sorption capacities (R_q).[8] The R_q values can be obtained by eqn (11).

$$R_q = \frac{q_{b,i}}{q_{m,i}} \tag{11}$$

where $q_{b,i}$ (mg g^{-1}) and $q_{m,i}$ (mg g^{-1}) are the uptake amounts of pollutant i in a binary system and mono-pollutant system with the same initial concentration, respectively. As is reported: (a) if $R_q > 1$, the uptake of pollutant i is enhanced by the co-existing pollutants, (b) if $R_q = 1$, co-existing pollutants have no influence on adsorption of pollutant i, and (c) if $R_q < 1$, the co-existing pollutants restrain the adsorption of pollutant i.[70]

The plotting of R_q values as a function of the initial MO or Cr(VI) concentrations is shown in Fig. 6(c and d). It is clear that
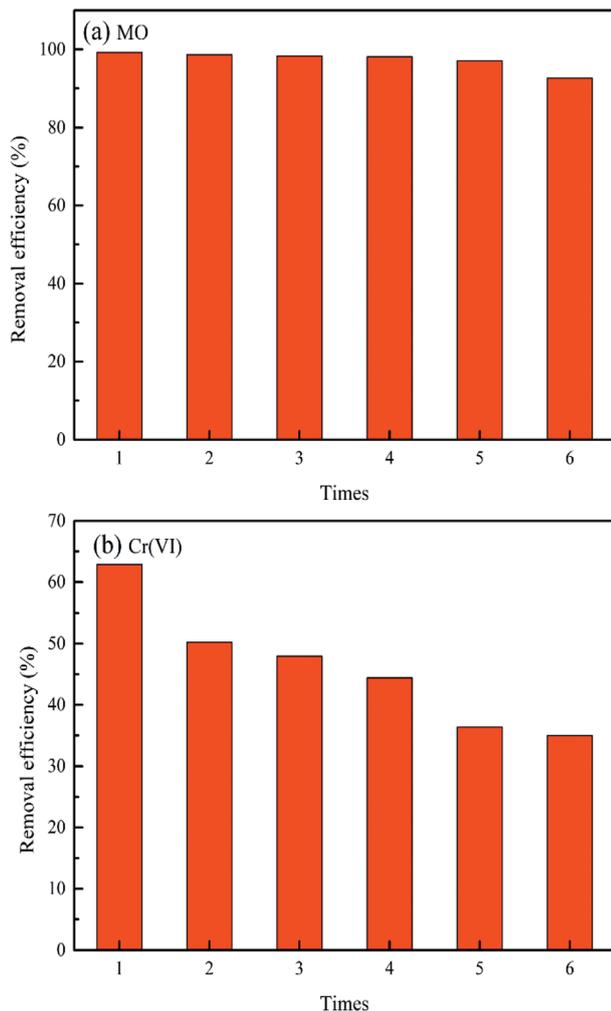
Fig. 5 Regeneration and stability studies of MO and Cr(VI) on MWCNTs@Fe$_3$O$_4$/PEI with six cycles (conditions: initial dye concentration, 200 mg L^{-1} for MO, 50 mg L^{-1} for Cr(VI); adsorbent dosage, 15 mg; solution pH, 3; contact time, 6 h for MO, 4 h for Cr(VI); temperature, 25 °C; and agitation speed, 150 rpm).

the R_q values of MO were respectively in the range of 0.5085 < R_q<0.5812 ([Cr(VI)]$_{co-existing}$ = 10 mg L^{-1}), and 0.3802 < R_q<0.4626 ([Cr(VI)]$_{co-existing}$ = 20 mg L^{-1}), suggesting that the presence of Cr(VI) suppressed the adsorption of MO due to the simultaneous uptake of MO and Cr(VI) by MWCNTs@Fe$_3$O$_4$/PEI. Interestingly, the adsorption of Cr(VI) was significantly increased with increasing concentration of MO in the MO-Cr(VI) binary system (i.e., 0.8653 < R_q < 1.2607 for Cr(VI) by the presence of MO with a concentration of 20 mg L^{-1}). This synergic effect may be ascribed to the fact that the MO molecules adsorbed onto MWCNTs@Fe$_3$O$_4$/PEI would provide a positively charged N-containing groups for Cr(VI) binding. It was previously evidenced that nitrogen-containing groups would be able to capture metals from aqueous solution.[71] This similar synergetic sorption performance was also reported by Tovar-Gómez et al. for the simultaneous removal of acid blue 25 and heavy metals from water using a Ca(PO$_3$)$_2$-modified carbon.[72] Overall, both Cr(VI) and MO could be simultaneously removed from Cr(VI)-MO

binary system by the as-synthesized adsorbent via multiple mechanisms such as electrostatic attraction, hydrogen bonding, π–π EDA interaction, manifesting that MWCNTs@Fe$_3$O$_4$/PEI composite is a promising adsorptive material in the treatment of combined pollution wastewater.

Adsorption confirmation by FT-IR, EDS and XPS spectra

In order to verify the occurrence of the adsorption process, the EDS and XPS spectra of the resulting adsorbent before and after target adsorbates adsorption were conducted, the results are shown in Fig. S5 and S6†, respectively. From the EDS spectra (shown in Fig. S5†), the new peaks corresponding to S and Cr could be observed in MO-loaded and Cr(VI)-loaded MWCNTs@Fe$_3$O$_4$/PEI, respectively, confirming the successful adsorption of MO and Cr(VI) by MWCNTs@Fe$_3$O$_4$/PEI. The peaks of S and Cr appear simultaneously in MO + Cr(VI)-loaded MWCNTs@Fe$_3$O$_4$/PEI, indicating the simultaneous removal of the as-prepared adsorbent of MO and Cr(VI). From the survey scan of XPS spectra (Fig. S5†), new peaks at around 166 eV due to S 2p and at around 586 eV ascribing to Cr 2p were observed in MO loaded and Cr(VI) loaded adsorbent, indicating the successful adsorption of MO or Cr(VI). The simultaneous adsorption of MO and Cr(VI) can also be verified by the appearance of peaks for both MO and Cr(VI) in MO + Cr(VI) loaded adsorbent.

In addition, after adsorption of MO and Cr(VI), the characteristic FTIR (Fig. 2b) peak at 1109.9 cm^{-1}, 825.5 cm^{-1} which belong to the C–N stretch and the characteristic FT-IR peak at 1027.8 cm^{-1} which belongs to the sulfonic acid ions stretch, indicating that MO has been successfully anchored onto the surface of the MWCNTs@Fe$_3$O$_4$/PEI. These changes in EDX, XPS and FT-IR spectra after adsorption confirmed that the amine groups of PEI have an important role in the capture of these two anionic pollutants.

Evaluation of MWCNTs@Fe$_3$O$_4$/PEI for model textile effluent treatment

A model textile effluent with 200 mg L^{-1} of MO or 50 mg L^{-1} of Cr(VI) was applied to evaluate the practical performance of the as-prepared MWCNTs@Fe$_3$O$_4$/PEI adsorbent in the present work. As shown in Fig. S7†, a relatively satisfactory removal efficiency of 96.1% for MO and 49.0% for Cr(VI) (compared with a removal rate of 99.2% for MO and 62.9% for Cr(VI) in deionized water system) by MWCNTs@Fe$_3$O$_4$/PEI can be still achieved. The slightly decreased removal rates of MO and Cr(VI) in model effluents were mainly due to the complexity of the matrix, which interferes with the adsorption of the target pollutants. Noticeably, the magnetically recyclable adsorbent can be easily regenerated and reused for model wastewater treatment without significant efficiency losses after several sorption-desorption runs. These results suggests that MWCNTs@Fe$_3$O$_4$/PEI can be considered as a qualified adsorbent for removing co-existing anionic organic and inorganic pollutants in industrial wastewater.
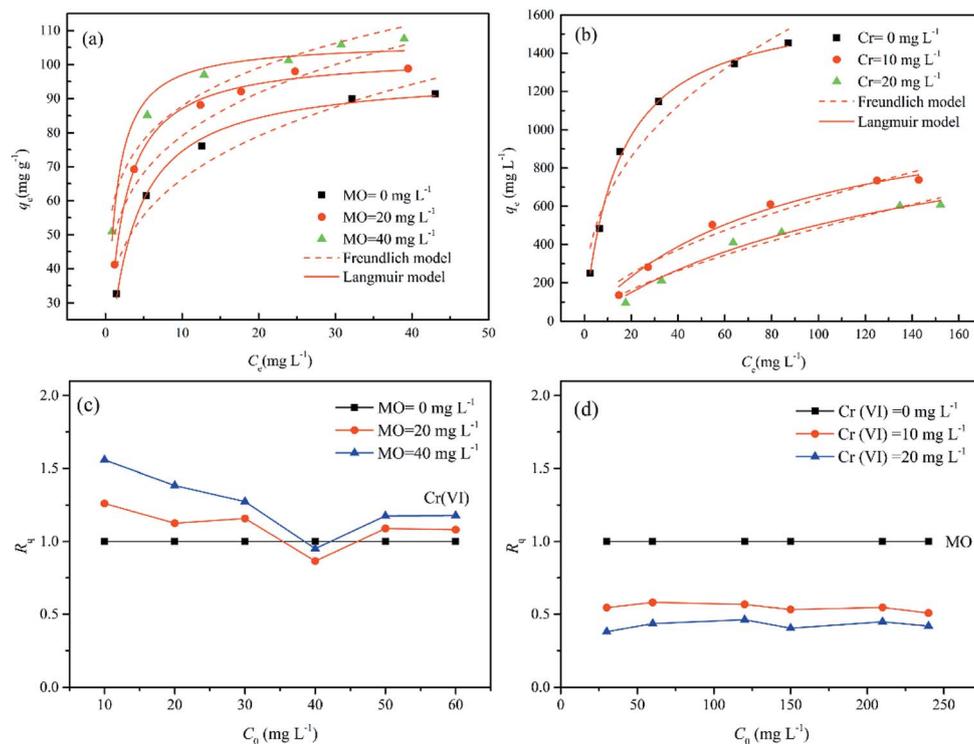
Fig. 6 Adsorption isotherms of Cr(VI) (a) and MO (b) by MWCNTs@Fe$_3$O$_4$/PEI in MO-Cr(VI) binary system. (Conditions: initial dye concentration, 30–240 mg L^{-1} for MO, 10–60 mg L^{-1} for Cr(VI); adsorbent dosage, 3 mg for MO, 10 mg for Cr(VI); solution pH, 3; contact time, 6 h for MO, 4 h for Cr(VI); temperature, 25–55 °C; and agitation speed, 150 rpm.)

Conclusions

In the present work, PEI decorated magnetic carbon nanotubes (MWCNTs@Fe$_3$O$_4$/PEI) were successfully synthesized using a facile method for use as a magnetically recyclable adsorbent to adsorb MO and Cr(VI) from aqueous solution. In a single-pollutant system, the uptake process of both MO and Cr(VI) by the resulting material follows a pseudo-second-order model and has a Langmuir isotherms model with q_e values of 1727.6 mg g^{-1} for MO and 98.8 mg g^{-1} for Cr(VI) at room temperature. The thermodynamic process of MO and Cr(VI) adsorption is spontaneous and endothermic in nature. In the MO-Cr(VI) binary system, the removal efficiency of Cr(VI) was greatly promoted by the presence of MO and the improving effect was highly dependent on the content of the coexisting MO to that of the protonated –N(CH$_3$)$_2$ portion of MO, which could provide additional sorption sites for Cr(VI) uptake. In contrast, owing to competition from Cr(VI) with a smaller molecular size with MO molecules, adsorption of MO was obviously restrained by the presence of Cr(VI). Interestingly, both MO and Cr(VI) could be simultaneously adsorbed from their mixture solutions (electrostatic interaction, π–π EDA interaction, and hydrogen bond for MO; electrostatic interaction and hydrogen bond for Cr(VI), both MO and Cr(VI)), suggesting its great potential in the treatment of complex real wastewater. Additionally, the as-prepared adsorbent showed excellent regeneration and stability for consecutive adsorption–desorption cycles. Therefore, the magnetically recyclable adsorbent could be considered as an excellent integrative adsorbent for the purification of actual wastewater contaminated by MO and Cr(VI). This work provides some insights into the design of an efficient and easily recyclable adsorbent for the simultaneous and synergetic removal of both organic and inorganic pollutants in complex wastewater.

Conflicts of interest

There are no conflicts to declare.

Acknowledgements

Notes and references

1 D. Pokhrel and T. Viraraghavan, *Sci. Total Environ.*, 2004, **333**, 37–58.
2 S. Zeng, S. Duan, R. Tang, L. Li, C. Liu and D. Sun, *Chem. Eng. J.*, 2014, **258**, 218–228.
3 H. Sun, L. Cao and L. Lu, *Nano Res.*, 2011, **4**, 550–562.
4 A. K. Sinha, M. Pradhan, S. Sarkar and T. Pal, *Environ. Sci. Technol.*, 2013, **47**, 2339–2345.
5 H. Zollinger, *Color Chemistry: Syntheses, Properties, and Applications of Organic Dyes and Pigments*, 2004.

6 Y.-Y. Chen, S.-H. Yu, H.-F. Jiang, Q.-Z. Yao, S.-Q. Fu and G.-T. Zhou, *Appl. Surf. Sci.*, 2018, **444**, 224–234.

7 J. Li, Q. Fan, Y. Wu, X. Wang, C. Chen, Z. Tang and X. Wang, *J. Mater. Chem. A*, 2016, **4**, 1737–1746.

8 F. Zhao, E. Repo, D. Yin, Y. Meng, S. Jafari and M. Sillanpää, *Environ. Sci. Technol.*, 2015, **49**, 10570–10580.

9 M. A. P. Cechinel, D. A. Mayer, L. P. Mazur, L. G. M. Silva, A. Girardi, V. J. P. Vilar, A. A. U. de Souza and S. M. A. G. U. de Souza, *J. Cleaner Prod.*, 2018, **172**, 1928–1945.

10 L. C. Tan, S. Papirio, V. Luongo, Y. V. Nancharaiah, P. Cennamo, G. Esposito, E. D. van Hullebusch and P. N. L. Lens, *Chem. Eng. J.*, 2018, **345**, 545–555.

11 X. Xiao, T.-T. Li, X.-R. Lu, X.-L. Feng, X. Han, W.-W. Li, Q. Li and H.-Q. Yu, *Bioresour. Technol.*, 2018, **251**, 204–209.

12 M. M. Matlock, B. S. Howerton and D. A. Atwood, *Water Res.*, 2002, **36**, 4757–4764.

13 F. Fu, L. Xie, B. Tang, Q. Wang and S. Jiang, *Chem. Eng. J.*, 2012, **189–190**, 283–287.

14 X. Wang, Z. Wang, H. Chen and Z. Wu, *J. Hazard. Mater.*, 2017, **339**, 182–190.

15 B. Ren, W. Shen, L. Li, S. Wu and W. Wang, *Appl. Surf. Sci.*, 2018, **447**, 711–723.

16 X. Li, D. Chen, N. Li, Q. Xu, H. Li, J. He and J. Lu, *Appl. Catal., B*, 2018, **229**, 155–162.

17 Y. Huang, X. Lee, F. C. Macazo, M. Grattieri, R. Cai and S. D. Minteer, *Chem. Eng. J.*, 2018, **339**, 259–267.

18 L. Cui, Y. Wang, L. Gao, L. Hu, L. Yan, Q. Wei and B. Du, *Chem. Eng. J.*, 2015, **281**, 1–10.

19 E. Ghasemi, A. Heydari and M. Sillanpää, *Microchem. J.*, 2017, **131**, 51–56.

20 W. Stawiński, A. Węgrzyn, O. Freitas, L. Chmielarz, G. Mordarski and S. Figueiredo, *Sci. Total Environ.*, 2017, **576**, 398–408.

21 Z. Wu, H. Zhong, X. Yuan, H. Wang, L. Wang, X. Chen, G. Zeng and Y. Wu, *Water Res.*, 2014, **67**, 330–344.

22 R. He, Z. Wang, L. Tan, Y. Zhong, W. Li, D. Xing, C. Wei and Y. Tang, *Microporous Mesoporous Mater.*, 2018, **257**, 212–221.

23 W. Yang, J. Wang, Q. Yang, H. Pei, N. Hu, Y. Suo, Z. Li, D. Zhang and J. Wang, *Chem. Eng. J.*, 2018, **339**, 230–239.

24 J. Jin, S. Li, X. Peng, W. Liu, C. Zhang, Y. Yang, L. Han, Z. Du, K. Sun and X. Wang, *Bioresour. Technol.*, 2018, **256**, 247–253.

25 E. N. Zare, A. Motahari and M. Sillanpää, *Environ. Res.*, 2018, **162**, 173–195.

26 L. Maggini, J.-M. Raquez, R. Marega, J. Jensen Ahrens, F. Pineux, F. Meyer, P. Dubois and D. Bonifazi, *ChemSusChem*, 2013, **6**, 367–373.

27 W. Chi, H. Shi, W. Shi, Y. Guo and T. Guo, *J. Hazard. Mater.*, 2012, **227–228**, 243–249.

28 D. Shan, S. Deng, C. He, J. Li, H. Wang, C. Jiang, G. Yu and M. R. Wiesner, *Chem. Eng. J.*, 2018, **332**, 102–108.

29 K. Yang, Z. Lou, R. Fu, J. Zhou, J. Xu, S. A. Baig and X. Xu, *J. Mol. Liq.*, 2018, **260**, 149–158.

30 M. Alizadeh Fard and B. Barkdoll, *J. Mol. Liq.*, 2018, **249**, 193–202.

31 L. Liu, D. Li, C. Li, R. Ji and X. Tian, *J. Hazard. Mater.*, 2018, **351**, 206–214.

32 F. Yu, J. Ma and S. Han, *Sci. Rep.*, 2015, **4**, 5326.

33 S. Li, Y. Gong, Y. Yang, C. He, L. Hu, L. Zhu, L. Sun and D. Shu, *Chem. Eng. J.*, 2015, **260**, 231–239.

34 X.-F. Sun, S.-G. Wang, W. Cheng, M. Fan, B.-H. Tian, B.-Y. Gao and X.-M. Li, *J. Hazard. Mater.*, 2011, **189**, 27–33.

35 B. Liu and Y. Huang, *J. Mater. Chem.*, 2011, **21**, 17413.

36 W. Maketon, C. Z. Zenner and K. L. Ogden, *Environ. Sci. Technol.*, 2008, **42**, 2124–2129.

37 X. Jin, Z. Xiang, Q. Liu, Y. Chen and F. Lu, *Bioresour. Technol.*, 2017, **244**, 844–849.

38 X. Sun, J. H. Chen, Z. Su, Y. Huang and X. Dong, *Chem. Eng. J.*, 2016, **290**, 1–11.

39 M. Owlad, M. K. Aroua and W. M. A. Wan Daud, *Bioresour. Technol.*, 2010, **101**, 5098–5103.

40 D. Shu, F. Feng, H. Han and Z. Ma, *Chem. Eng. J.*, 2017, **324**, 1–9.

41 C. Liu, R. Jin, X. Ouyang and Y. Wang, *Appl. Surf. Sci.*, 2017, **408**, 77–87.

42 D. Xiao, P. Dramou, H. He, L. A. Pham-Huy, H. Li, Y. Yao and C. Pham-Huy, *J. Nanopart. Res.*, 2012, **14**, 984.

43 E. E. Arthur, F. Li, F. W. Y. Momade and H. Kim, *Energy*, 2014, **76**, 822–829.

44 L. Wang and L. Gao, *J. Phys. Chem. C*, 2009, **113**, 15914–15920.

45 B. Chen, Y. Liu, S. Chen, X. Zhao, W. Yue and X. Pan, *Environ. Sci.: Nano*, 2016, **3**, 670–681.

46 Y. Ren, H. A. Abbood, F. He, H. Peng and K. Huang, *Chem. Eng. J.*, 2013, **226**, 300–311.

47 L. Fan, C. Luo, Z. Lv, F. Lu and H. Qiu, *J. Hazard. Mater.*, 2011, **194**, 193–201.

48 J. Xiao, W. Lv, Z. Xie, Y. Tan, Y. Song and Q. Zheng, *J. Mater. Chem. A*, 2016, **4**, 12126–12135.

49 M. Monier, D. M. Ayad, Y. Wei and A. A. Sarhan, *J. Hazard. Mater.*, 2010, **177**, 962–970.

50 N. M. Tomić, Z. D. Dohčević-Mitrović, N. M. Paunović, D. Ž. Mijin, N. D. Radić, B. V. Grbić, S. M. Aškrabić, B. M. Babić and D. V. Bajuk-Bogdanović, *Langmuir*, 2014, **30**, 11582–11590.

51 H. Y. Zhu, R. Jiang, Y.-Q. Fu, J.-H. Jiang, L. Xiao and G.-M. Zeng, *Appl. Surf. Sci.*, 2011, **258**, 1337–1344.

52 F. Liu, S. Teng, R. Song and S. Wang, *Desalination*, 2010, **263**, 11–17.

53 Z. Dong, D. Wang, X. Liu, X. Pei, L. Chen and J. Jin, *J. Mater. Chem. A*, 2014, **2**, 5034–5040.

54 S. Zhang, Y. Zhang, G. Bi, J. Liu, Z. Wang, Q. Xu, H. Xu and X. Li, *J. Hazard. Mater.*, 2014, **270**, 27–34.

55 X. Ruan, Y. Chen, H. Chen, G. Qian and R. L. Frost, *Chem. Eng. J.*, 2016, **297**, 295–303.

56 X. Li, Z. Wang, J. Ning, M. Gao, W. Jiang, Z. Zhou and G. Li, *J. Environ. Manage.*, 2018, **217**, 305–314.

57 J. Li, Z. Shao, C. Chen and X. Wang, *RSC Adv.*, 2014, **4**, 38192.

58 S. Bao, K. Li, P. Ning, J. Peng, X. Jin and L. Tang, *J. Taiwan Inst. Chem. Eng.*, 2018, **87**, 64–72.

59 Z. Li, Y. Sun, J. Xing, Y. Xing and A. Meng, *J. Hazard. Mater.*, 2018, **352**, 204–214.

60 L. Deng, Z. Shi, X. Peng and S. Zhou, *J. Alloys Compd.*, 2016, **688**, 101–112.

61 S. Shi, J. Yang, S. Liang, M. Li, Q. Gan, K. Xiao and J. Hu, *Sci. Total Environ.*, 2018, **628–629**, 499–508.

62 K. Zhu, C. Chen, H. Xu, Y. Gao, X. Tan, A. Alsaedi and T. Hayat, *ACS Sustainable Chem. Eng.*, 2017, **5**, 6795–6802.

63 L. Deng, Z. Shi, L. Wang and S. Zhou, *J. Phys. Chem. Solids*, 2017, **104**, 79–90.

64 L. Luo, W. Cai, J. Zhou and Y. Li, *J. Hazard. Mater.*, 2016, **318**, 452–459.

65 X. Tian, W. Wang, Y. Wang, S. Komarneni and C. Yang, *Microporous Mesoporous Mater.*, 2015, **207**, 46–52.

66 S. Hozhabr Araghi, M. H. Entezari and M. Chamsaz, *Microporous Mesoporous Mater.*, 2015, **218**, 101–111.

67 D. Xu, K. Zhu, X. Zheng and R. Xiao, *Ind. Eng. Chem. Res.*, 2015, **54**, 6836–6844.

68 J.-H. Huang, K.-L. Huang, S.-Q. Liu, A.-T. Wang and C. Yan, *Colloids Surf., A*, 2008, **330**, 55–61.

69 M. Ghaedi, B. Sadeghian, A. A. Pebdani, R. Sahraei, A. Daneshfar and C. Duran, *Chem. Eng. J.*, 2012, **187**, 133–141.

70 V. Hernández-Montoya, M. A. Pérez-Cruz, D. I. Mendoza-Castillo, M. R. Moreno-Virgen and A. Bonilla-Petriciolet, *J. Environ. Manage.*, 2013, **116**, 213–221.

71 J. Zhang, S. Zhai, S. Li, Z. Xiao, Y. Song, Q. An and G. Tian, *Chem. Eng. J.*, 2013, **215–216**, 461–471.

72 R. Tovar-Gómez, D. A. Rivera-Ramírez, V. Hernández-Montoya, A. Bonilla-Petriciolet, C. J. Durán-Valle and M. A. Montes-Morán, *J. Hazard. Mater.*, 2012, **199–200**, 290–300.